Chapter 2

Hadron-Hadron Scattering

In a high energy proton-proton collision we can have either soft or hard processes. Most of the time the hard processes are accompanied by soft interactions, occurring along the hadron interaction. While the hard processes as the Higgs boson production, or the high p_T jet production are well understood using perturbative QCD, the soft processes as the underlying event, the hadronization are not so well understood. In fact, these processes involving a low energy scale at which perturbative series expansion of QCD breaks down, are studied with non perturbative approaches.

This chapter gives a theoretical introduction on some basic elements of perturbative QCD theory: the QCD factorization theorem, the fixed-order approach in perturbative QCD calculations, and finally the all-orders approaches (e.g. the parton showers).

2.1 QCD factorization theorem

The fundamental idea for the description of a hadron-hadron collision is that hadrons are made-up from partons that, at some high energy scale, can be seen as free. So the hadron-hadron interaction can be seen as an interaction between two free partons, given a sufficiently high energy scale for the interaction.
This idea was developed in the framework of the deep inelastic scattering, and the Bjorken scaling observation confirms it [2]. The generalization of this concept leads to the QCD factorization theorem.
The factorization theorem was introduced first by Drell and Yan [3]. The hadron-hadron scattering cross-section is described in terms of partons extending the formalism used for deep inelastic scattering, through the following factorized formula:

$$\sigma_{AB} = \int dx_a \, dx_b \, f_{a/A}(x_a) \, f_{b/B}(x_b) \, \hat{\sigma}_{ab\to X} \quad . \tag{2.1}$$

Where X is a partonic/leptonic state and $a\,(b)$ a quark or an antiquark in the hadron $A\,(B)$. The σ_{AB} is the hadronic cross-section while $\sigma_{ab\to X}$ is the partonic cross section that can be calculated using perturbative QCD. Finally, the $f_{a/A}\,(f_{b/B})$ is the parton distribution function in the hadron $A\,(B)$ that is dependent on $x_a\,(x_b)$ that is the momentum fraction of the total momentum of the hadron $A\,(B)$ carried

by the parton. This is valid in the "scaling" limit:

$$s \longrightarrow \infty \ , \qquad \frac{M_X}{\sqrt{s}} = \text{finite} \quad ; \tag{2.2}$$

where the center-of-mass energy grows to infinity but with a fixed ratio of the X state invariant mass and the center-of-mass energy.
A problem arises from the perturbative corrections from real and virtual gluon emission, in particular from the collinear gluon emissions. These contributions take to a logarithmic divergence (spoiling the convergence of the perturbative expansion). These dependencies can be absorbed by the parton distribution functions (that evolve according the DGLAP equations). This results in the scaling violation of the parton distribution functions

$$f_{a/A}(x_a) \longrightarrow f_{a/A}(x_a, Q^2) \quad , \tag{2.3}$$

i.e. the parton distribution function depend not only on the momentum fraction x, but also on the energy scale Q^2 of the interaction.
So, we can rewrite the factorization theorem in Eq. 2.1 as:

$$\sigma_{AB} = \int dx_a \, dx_b \, f_{a/A}(x_a, Q^2) \, f_{b/B}(x_b, Q^2) \, \hat{\sigma}_{ab\to X} \quad . \tag{2.4}$$

At this point the *finite* corrections to the leading-logarithmic cross section in the perturbative expansion are specific for each process (i.e. they are not universal, but they are process dependent). This leads in the Eq. 2.4 to the following series in α_s (the coupling constant of QCD theory):

$$\sigma_{AB} = \int dx_a \, dx_b \, f_{a/A}(x_a, \mu_F^2) \, f_{b/B}(x_b, \mu_F^2) \, \left[\hat{\sigma}_0 + \alpha_s(\mu_R^2)\hat{\sigma}_1 + \dots\right] \quad . \tag{2.5}$$

In Eq. 2.5 two scales enter the formula:

- The *factorization scale* μ_F: this scale is related to the resolution with which the hadron is being probed, separates long- and short- distance physics processes.

- The *renormalization scale* μ_R: the scale at which is evaluated the strong coupling constant α_s. The dependence of α_s on the renormalization scale is related to different effects such as the vacuum polarization, the quark self-energy, the vertex corrections, and the gluon loop corrections to the elementary three-gluon and four-gluon couplings.

The higher-order corrections to the cross section in Eq. 2.5 are important because they lead to an higher accuracy in the cross section prediction, gradually reducing the dependencies on μ_R and μ_F. In absence of an all-order prediction, a choice for the two scales have to be taken. Typically, the scales are assumed to be equal: in the Drell-Yan process the standard choice is $\mu_F = \mu_R = M$, with M the lepton-pair mass [4]; other cases are the invariant masses of Z-boson, top quark or jet transverse energy to study [4] the production cross sections for Z-bosons, top quarks and large E_T jets respectively.

The parton distribution functions used to describe a hard scattering are solution to the DGLAP (Dokshitzer–Gribov–Lipatov–Altarelli–Parisi) equations [5, 6, 7, 8]

$$\mu_F^2 \frac{\partial f_{i/H}(x,\mu_F^2)}{\partial \mu_F^2} = \sum_j \frac{\alpha_s(\mu_F^2)}{2\pi} \int_x^1 \frac{dz}{z} P_{i\to j}(z)\ f_{j/p}\left(\frac{x}{z}, \mu_F^2\right) \quad , \tag{2.6}$$

where $P_{i\to j}$ are the so-called splitting functions: they are the probability that a parton of type i emits a parton j (a quark or a gluon) carrying a fraction z of the i-parton momentum.
The splitting functions have the following perturbative expansions in $alpha_s$:

$$P_{i\to j}(x,\alpha_s) = P^{(0)}_{i\to j}(x) + \frac{\alpha_s}{2\pi} P^{(1)}_{i\to j}(x) + \dots \quad . \tag{2.7}$$

This procedure has been used to calculate cross-sections for many Standard Model processes in $p\bar{p}$ and pp scattering respectively at Tevatron and LHC energies as shown in Fig. 2.1.

The parton distribution functions dependence on Q^2 can be derived theoretically via the DGLAP equations. Instead, the x dependence is obtained fitting the deep-inelastic and other hard-scattering processes experimental data. The experimental coverage in (x, Q^2)-plane is shown in Fig. 2.2 where is also underlined the relationship between (x, Q^2) and kinematic variables in Drell-Yan processes for a final state with invariant mass M and rapidity y (further details in section 2 of [4]). Assuming that the factorization scale Q is equal to M (The reference center of mass energy is 13 TeV), for two incoming partons with four-momentum respectively p_1 and p_2, the relations of their x (labeled as x_1 and x_2) with s, y and M are:

$$\begin{aligned} p_1^\mu &= \frac{\sqrt{s}}{2}(x_1, 0, 0, x_1) \\ p_2^\mu &= \frac{\sqrt{s}}{2}(x_2, 0, 0, -x_2) \end{aligned} \quad \Longrightarrow \quad x_1 = \frac{M}{\sqrt{s}} e^{y} \qquad x_2 = \frac{M}{\sqrt{s}} e^{-y} \quad , \tag{2.8}$$

where $s = (p_1^\mu + p_2^\mu)^2$. For example the figure shows that the production of a final state with invariant mass $M = 100$ GeV and rapidity $y = 2$ is given by the interaction of two hadrons with $x_1 \approx 0.05$ and $x_2 \approx 0.001$ with $Q^2 = 10^4$ GeV^2

2.2 Partonic cross-section

Partonic cross section as seen in Eq. 2.1 is one of the fundamental ingredients in our recipe for the description of hadron-hadron interactions. It can be calculated as a perturbative expansion in α_s from QCD first principles using quantum field theory. The calculation of such expansion at the leading order (LO) is performed by evaluating all the possible tree-level Feynman diagrams for every process. Then the calculation proceeds by computing the squared matrix element and by integrating it over the available phase space (analytically or numerically).
At this point, we can already encounter some divergence that can be avoided imposing some restrictions on the phase space.

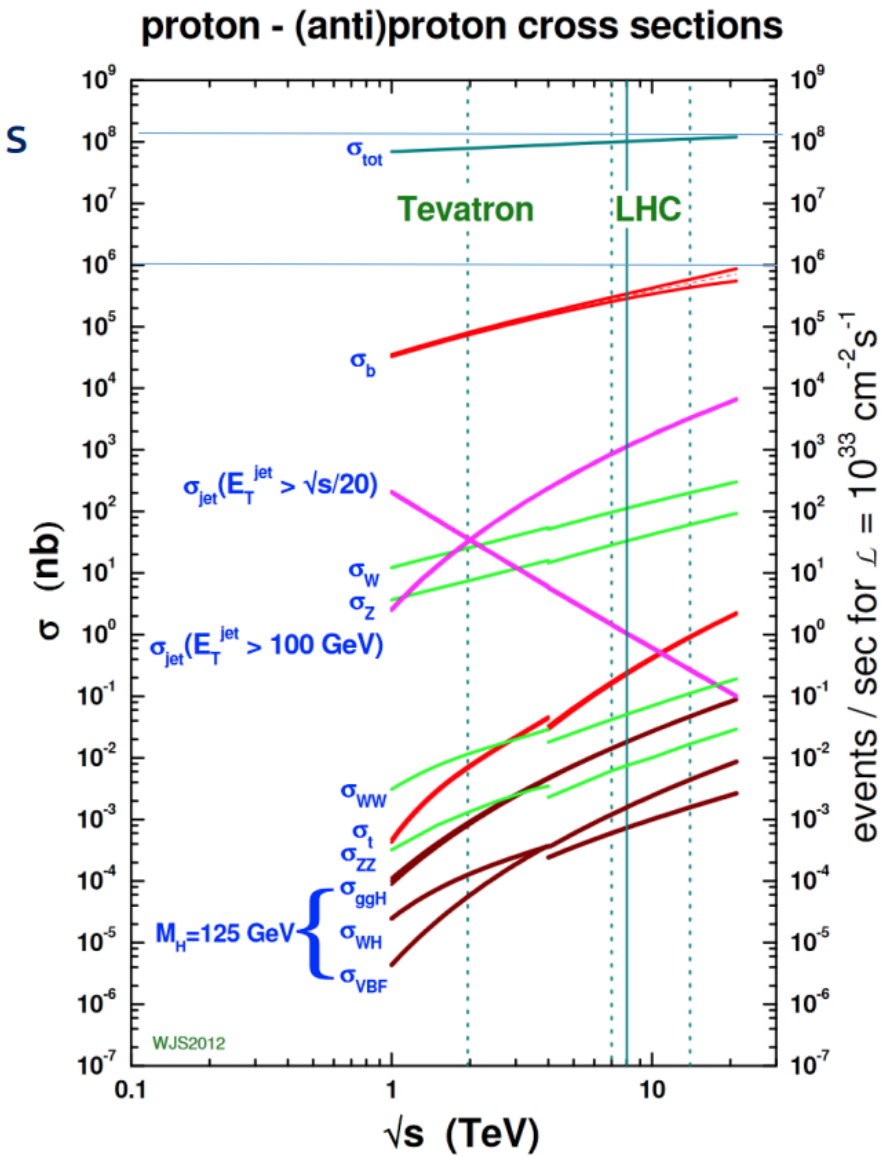

Figure 2.1: Next-to-leading order cross sections at Tevatron and LHC colliders energies (the splitting are at the transition between $p\bar{p}$ and pp cross section). Figure from [9]

2.2.1 Higher order calculations

The LO calculation can describe broad feature of a particular process and provide a first estimation of its cross section; anyway, in many cases this is insufficient.
The main source of uncertainty derives from the LO dependence on the unphysical renormalization and factorization scales. Some process may contribute only when going beyond the first approximation, and some divergence can be resummed.
The next-to-leading order (NLO) calculation requires all the Feynman diagrams that take an extra α_s. This contribution can arise in two different ways:

- **Virtual**: internal lines in the Feynamn diagram, see Fig. 2.3a, that don't originate a real particle in the initial or in the final state (loops);
- **Real**: external lines int the Feynamn diagram, see Fig. 2.3b, here the particle

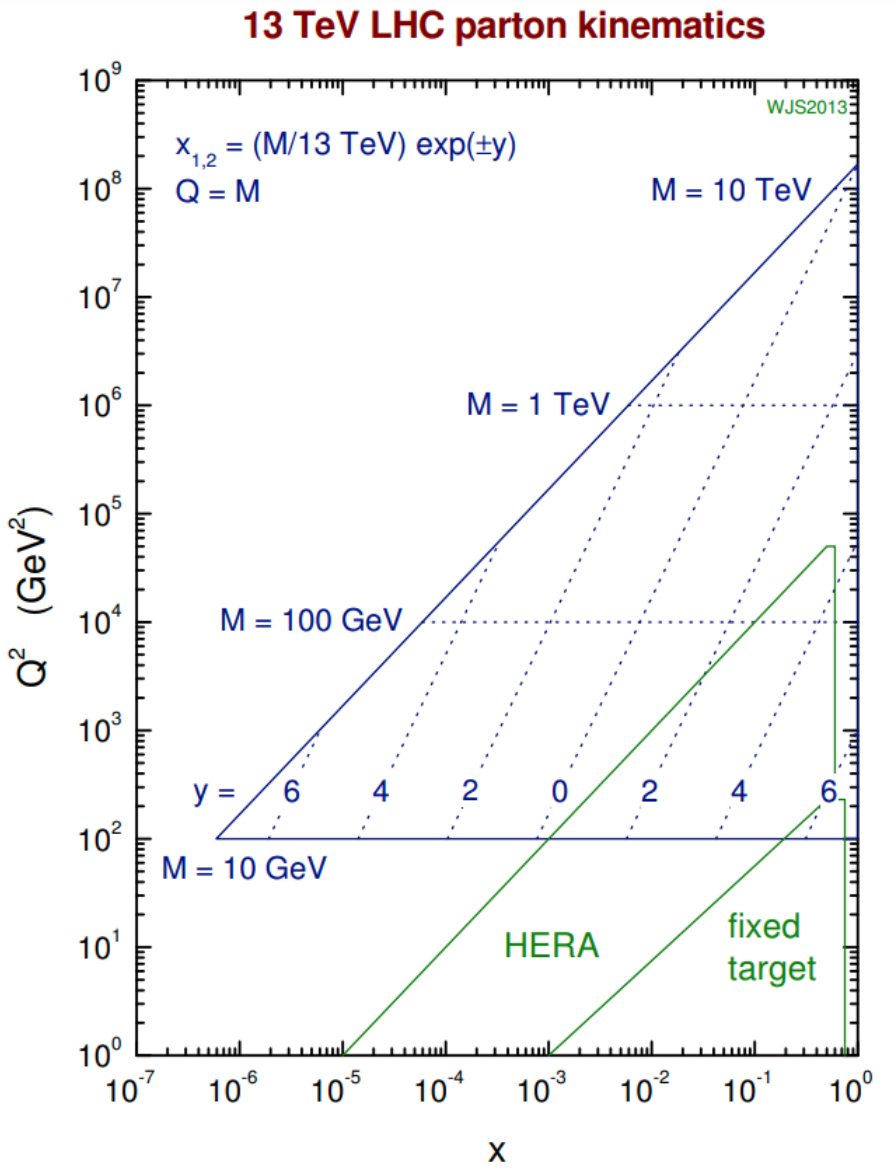

Figure 2.2: Graphical representation of the parton (x, Q^2) variables coverage of different experiments. For LHC these x and Q^2 are related to the kinematic variables y and M. Figure from [9]

is real and participate to the initial or final state observed (real particles).

Virtual corrections contains infrared divergences, arising by integrating on the loop circulating momentum, that cancel against infrared singularities given by collinear or soft emissions [10, 11, 12].
A common strategy for the renormalization is dimensional regularization: it consists into performing the calculation in a $D = 4 - 2\epsilon$ dimensional space ($\epsilon < 0$); in that way the singularities appear as single and double poles in ϵ. Then, the limit $\epsilon \to 0$ is taken after the divergences have cancelled.
This NLO calculation with regularization allows to extend the treatment of these integrals up to zero transverse momentum.

The importance of higher-order calculation is that it allows too describe more processes, as can be shown with the following example. In a Z boson production:

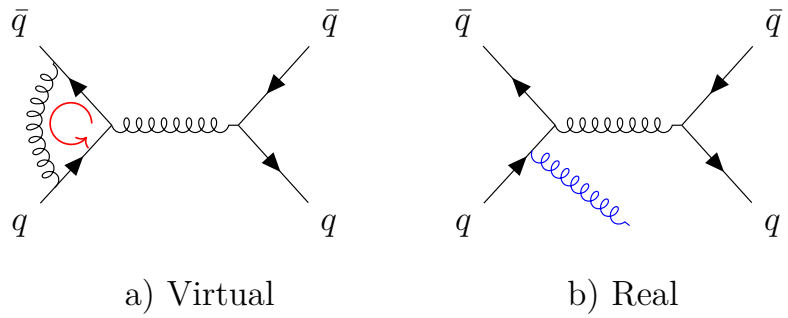

Figure 2.3: Feynamn diagrams for a virtual correction (a) the momentum circulating in the loop when integrated on the phase space take to a divergence; and a real correction (b) the particle emitted is real, participate to the initial or final state of the process.

1) **LO**: the Z is produced without transverse momentum (p_T), and anything can recoil against the Z for momentum conservation (Fig. 2.4a).

2) **NLO**: the Z acquires a finite p_T. In this case the Z boson p_T is balanced by a single parton/gluon (Fig. 2.4b).

3) **NNLO**: the Z p_T can be balanced by two jets (Fig. 2.4c).

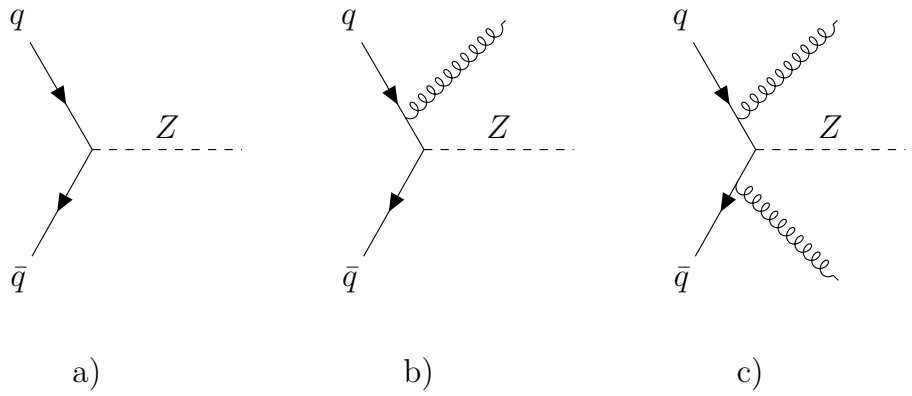

Figure 2.4: Feynman diagrams for the Z production by annihilation of a quark and an antiquark at LO (a), NLO (b), NNLO (c). At LO the Z can only be produced with a $p_T = 0$ for the conservation of the momentum.

Another important benefit of performing a NLO calculation is the the reduction of the dependence of calculation on the unphysical renormalization (μ_R) and factorization (μ_F) scales. It is proven that higher order calculations of observables calculated to order α_s^n are dependent upon the unphysical scales only at order higher than α_s^{n+1} [4]. The range of predictions corresponding to different scale choices is usually attributed to *theoretical uncertainties*, as is shown in Fig. 2.5, where the uncertainties reduce from the LO calculation to the NLO and even more to the NNLO.

2.3 Parton Showers

A different approach to describe the phenomena observed at high-energy colliders, instead of calculating cross sections order by order in the perturbative expansion, is

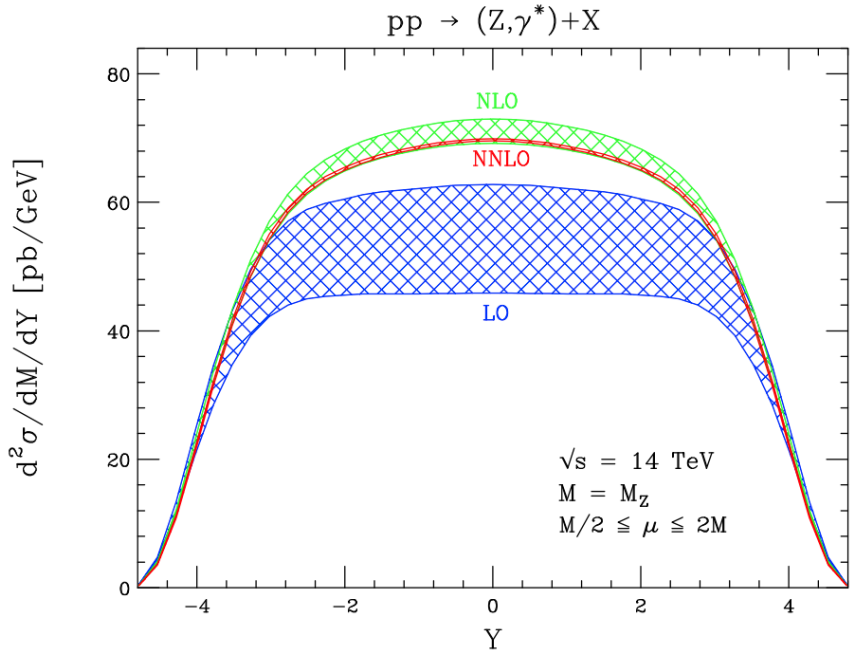

Figure 2.5: The rapidity distribution predictions at LO (blue) NLO (green) and NNLO (red) for the Z production at the center of mass energy $\sqrt{s} = 14$ TeV. The band width is related to the uncertainties. Going from LO to NLO there is a increase in the cross section prediction and a reduction on the scales uncertainties, the NNLO prediction is in the NLO error band width but there is a further increase in the precision of the prediction. Figure from [4], section 6.

the use of an *all-order* approach.
Different all-order approaches exist such as resummation techniques and parton showers. Resummation is based on the observation that in many quantities the smallness of the expansion coefficients α_s is violated by large logarithmic enhancements. This takes the dominant contribution from each order and "resums" them by means of an evolution equation. The main problem in QCD is related to the fact that lot of quantities have corrections of the form $\alpha_s^n \log^k(Q_i/Q_j)$ where Q_i and Q_j are two different energies scales, for example:

– Renormalization $\mu_R = Q^2$ and factorization scales logs: $\alpha_s^n \log^n(Q^2/\mu_f)$

Various methods to perform this resummation exist.
An example is the Z production p_T spectrum shown in Fig. 2.6: here the comparison between experimental CDF data and theoretical predictions is shown: in the low p_T region the *all-order* approach regularizes the divergence of the fixed order calculation and describes the data better.

An other *all-order* approach is based on the simulation of the so-called "parton showers". It is implemented in different Monte Carlo programs, as PYTHIA [14], HERWIG [15] and SHERPA [16]. The algorithm starts from few partons arising from a hard interaction. Then, as the energy scale at which we examines the scattering decrease these harder partons can split, and so more partons are produced in the shower. The higher scale parton are related to the lower energy scale (close to Λ_{QCD}) using the DGLAP evolution equation formalism. The solution to this equation can be written using a Sudakov form factor arising from the probability of no gluon

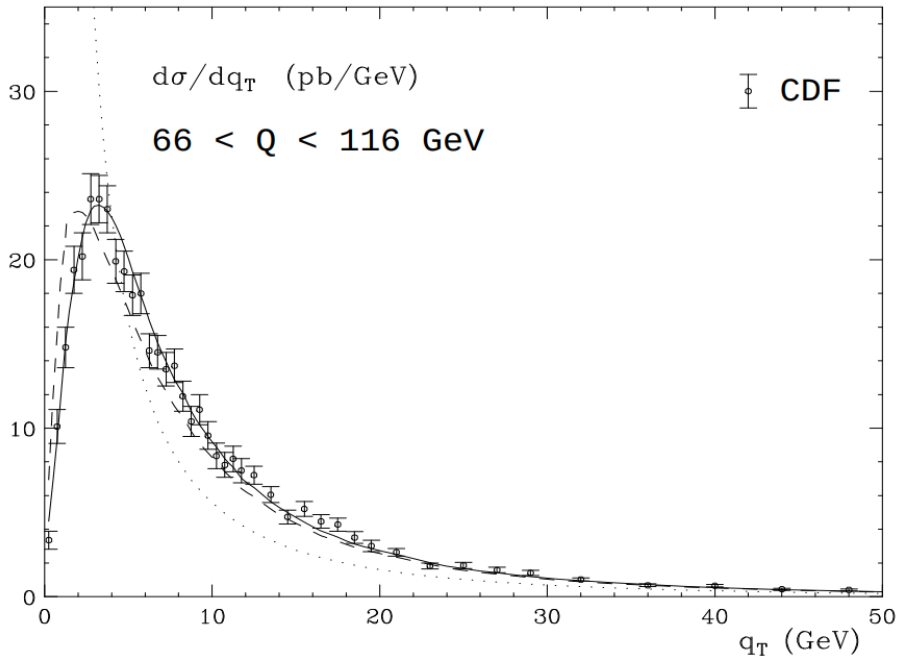

Figure 2.6: CDF data on Z production cross section at Tevatron collider, CDF experiment, the predictions from fixed order calculation (dotted) with resummation (dashed), and with the inclusion of power corrections (solid) are compared. Figure take from [13]

emission in the evolution from higher to lower scale.
In the parton showering process, in addition to the kinematic variables (momentum fraction z and azimuthal angle ϕ) and flavours of the partons, an evolution variable t is generated. PYTHIA8 uses as evolution variable the squared of the relative transverse momentum of the two partons in the splitting (p_T^2). Different choices are made in HERWIG and SHERPA.
As mentioned before, the shower evolution is based on the standard (LO) DGLAP splitting kernels P(z) described here:

$$P_{q\to qg}(z) = C_F \frac{1+z^2}{1-z} \quad ; \tag{2.9}$$

$$P_{g\to gg}(z) = C_A \frac{(1-z(1-z))^2}{z(1-z)} \quad ; \tag{2.10}$$

$$P_{q\to q\bar{q}}(z) = T_R(z^2+(1-z)^2) \quad ; \tag{2.11}$$

where $C_F = \frac{4}{3}$ is the Casimir operator for $SU(3)$, $C_A = N_C = 3$, that are named "color factors", and $T_R = \frac{1}{2}$ that is given by the trace calculation of the group generators, each contribution is multiplied by N_f if summing over all contributing quark flavours.
The parton shower consist of two components: the initial-state radiation (ISR) describing the emission from the incoming partons and the final-state radiation (FSR) describing emission of outgoing partons. Both ISR and FSR algorithms are based on these splitting kernels. The respective probabilities of emitting radiation

as one moves in the decreasing evolution variable sequence are:

$$FSR: \qquad \frac{d\mathcal{P}_{FSR}}{dp_T^2} = \frac{1}{p_T^2}\int \frac{dz}{z}\frac{\alpha_s}{2\pi}P(z) \quad ; \tag{2.12}$$

$$ISR: \qquad \frac{d\mathcal{P}_{ISR}}{dp_T^2} = \frac{1}{p_T^2}\int \frac{dz}{z}\frac{\alpha_s}{2\pi}P(z)\frac{f'(x/z,p_T^2)}{f(x,p_T^2)} \quad . \tag{2.13}$$

We can write-out our Sudakov form factor by using the two probability in Eq. 2.12 and Eq. 2.13, as

$$\Delta(p_T^2) = \exp\left(-\int_{p_T 0}^{p'_T}\frac{d\mathcal{P}_{PS}}{dp_T^2}\,dp_T\right) \qquad \text{with} \quad PS = ISR,\ FSR \quad . \tag{2.14}$$

The Sudakov form factor give the probability of a parton to evolve from an harder scale to a softer scale without emitting a parton harder than some resolution scale. The introduction of the Sudakov form factor resums all the effects from the soft and collinear gluon emission. For more details and some plots of different Sudakov form factor values see section 3.5 of [4].

2.3.1 Merging parton showers and matrix element calculations

Regions dominated by soft and collinear gluon emissions are described very well by parton showers approach; on the other hand, regions where partons are energetic and widely separated are well described by matrix element calculations. So, the best approach would be to combine the two different descriptions, this would require an universal formalism for parton showers and matrix element calculations. This universal formalism was created in 2001 and it is called "Les Houches Accord" [17]. In order to combine the two approaches some care must be taken: there is the risk of double counting. Different techniques prevent this risk: for example CKKW [18] is used to combine LO matrix element calculations and parton shower.

A better way is to combine NLO matrix element calculation with parton showers: this is done by the FxFx mergin scheme, developed by Frixione, Nason, Webber in the MC@NLO framework [19, 20, 21, 22]. In this scenario the risk of double counting is given by the fact that at NLO one emission can be made explicit as indicated in Fig. 2.7 by the red gluon line, then the progress of the parton shower can leads to a double counting between real emission matrix element and the parton shower as shown in Fig. 2.7, the double counting sources are indicated by the blue arrows.

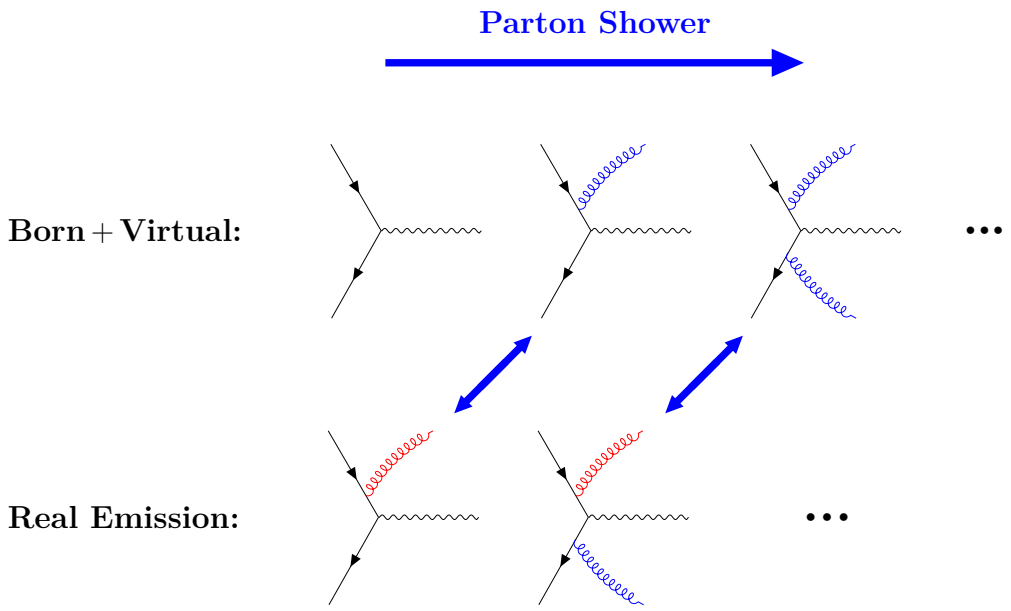

Figure 2.7: The FxFx margin scheme have to avoid this double counting. Feynman diagrams that can lead to a double counting are grouped with the violet arrow, the blue emission are related to the parton shower while the red ones to the NLO process.

2.4 Parton distribution functions

The last ingredient in our recipe is the knowledge of the quark and gluon distributions inside the two hadrons that undergo the scattering. We have already seen that these quantities are depending on the virtuality (Q^2) of the interaction.
The information on the quark distribution inside a hadron $f_{q/p}(x, Q^2)$ arises from lepton-hadron DIS experiments, from lepton-pair production in hadron-hadron collisions (Drell-Yan processes) and jet measurements to study gluon distribution $f_{g/p}(x, Q^2)$. All these quantities are the experimental input in order to evaluate the PDF inside the hadron while the Q-evolution is described by DGLAP equation. The evolution of the PDF can be run either with a NLO or with a NNLO calculations.

The kinematic region covered by experiments is shown in Fig. 2.2. At very low x and Q^2 the DGLAP evolution is believed to be no longer applicable and a BFKL (Balitsky-Fadin-Kuraev-Lipatov) [23, 24] description must be used.
A lot of processes are available for the PDFs evaluation and a lot of PDF set have been generated, as an example Fig. 2.8 shows the NNPDF3.1 set [25] at NNLO for a virtuality $Q^2 = 10$ GeV^2 (left) and $Q^2 = 10^4$ GeV^2 (right). Note that the gluon contribution have been scaled of a factor 10: in fact, in the low x region, $x < 0.01$, the gluon contribution is the dominating one, while at high x value the valence quarks dominate the PDF.
In Fig. 2.8 we can also see that with increasing virtuality (Q^2) at low x the density of the sea quarks increases: this is related to the fact that our hadrons are probed at higher energy and the probe resolution is proportional to the energy.

$$\text{Resolution} \sim \frac{\hbar}{Q} \quad . \tag{2.15}$$

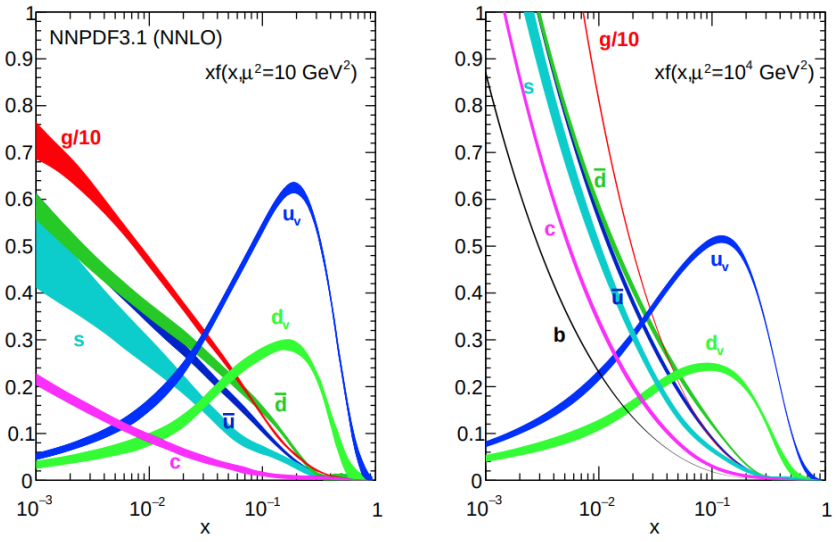

Figure 2.8: The NNPDF3.1 NNLO PDFs set, evaluated at $Q^2 = 10$ GeV^2 (left) and $Q^2 = 10^4$ GeV^2 (right). At low x the contribution from the gluons is the dominating one while at higher x the dominant contribution is from the valence quarks. The PDF Q evolution shows that when our proton is probed to higher Q^2 the resolution increase (higher Q correspond to smaller distance resolution) and so we have a bigger contribution from the sea quarks at low x values.

So, when probed at higher energy, the hadrons appear denser[1] than when are probed at lower energy. This, as will be discussed in the next chapter, is related to the higher number of interaction between partons in a single hadron-hadron collision. The phenomenon of having more than one interaction between partons in a single hadron-hadron collision is called *multiple parton interaction*: this concept will be discussed in the next chapter.

2.5 A real proton-proton collision

We have understood that the complexity in the description of a proton-proton collision arises from composite nature of the protons. In this chapter we discussed the importance of the QCD factorization theorem that help us in the calculation of the hadronic cross section with the convolution between the partonic cross section and the parton distribution functions (PDF). We have discussed the importance of the parton shower algorithm where a set of partons are evolved in a more complex final state by emissions in the initial and final states.
All these processes are important in the description of a real proton-proton collision but also the partons that are left unscattered are non-color singlet and can contribute to the complex final state observed in the experiments, and additionally, as mentioned before, nothing prevent additional partons scatterings from taking place and increasing more and more the complexity of the partons final state.

[1] This density growth is not endless but at some point a saturation is reached it is called *parton saturation*. The parton saturation find an explanation in the observation that at some high energy scale the parton mergers have to eventually compensate for splittings.

Another problem is related to the not-well-understood hadronization process of all the final-state partons involved in the hadron-hadron interaction. Hadronization is not known from first principles and different models have been implemented in different programs: the *cluster fragmentation model* implemented in HERWIG and the *string fragmentation model* in PYTHIA All these processes are schematically shown in Fig. 2.9.

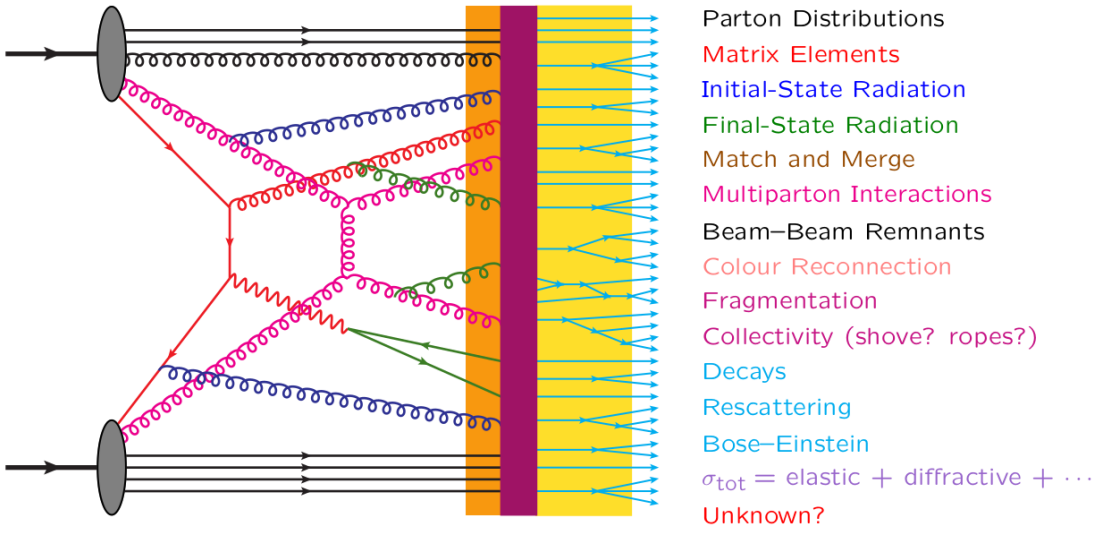

Figure 2.9: A schematic representation for a *pp* collision. Reading the image from left to right one can have an idea on the evolution of the system. The two incoming hadrons enter the scattering from the left side, the red line indicate the main hard scattering and the magenta one the second parton scattering (MPI) each interaction is associated with initial (blue) and final (green) state radiation, the unscattered partons (black lines) re-enter the color reconnection and hadronization processes. Than the new formed hadrons (lightblue) can undergo to different decays.

Next chapter will describe in more details the PYTHIA Monte Carlo generator, that is currently used to simulate many processes in proton-proton collision at the LHC. PYTHIA introduces different free parameters that need to be tuned with experimental data (from Tevatron and LHC). The tune methods are described in Chapter 5 along with the description of some already existing tune for the underlying event in proton-proton collision.

Bibliography

[1] Steven Weinberg. A model of leptons, Nov 1967. URL https://link.aps.org/doi/10.1103/PhysRevLett.19.1264.

[2] J. D. Bjorken. Asymptotic Sum Rules at Infinite Momentum. *Phys. Rev.*, 179: 1547–1553, 1969. doi: 10.1103/PhysRev.179.1547.

[3] Sidney D Drell and Tung-Mow Yan. Partons and their applications at high energies, 1971. ISSN 0003-4916. URL https://www.sciencedirect.com/science/article/pii/0003491671900716.

[4] J M Campbell, J W Huston, and W J Stirling. Hard interactions of quarks and gluons: a primer for lhc physics, Dec 2006. ISSN 1361-6633. URL http://dx.doi.org/10.1088/0034-4885/70/1/R02.

[5] L N Lipatov. The parton model and perturbation theory, 1975. URL http://cds.cern.ch/record/400357.

[6] Vladimir Naumovich Gribov and L N Lipatov. Deep inelastic ep scattering in perturbation theory, 1972. URL https://cds.cern.ch/record/427157.

[7] G. Altarelli and G. Parisi. Asymptotic freedom in parton language, 1977. ISSN 0550-3213. URL https://www.sciencedirect.com/science/article/pii/0550321377903844.

[8] Yuri L. Dokshitzer. Calculation of the Structure Functions for Deep Inelastic Scattering and e+ e- Annihilation by Perturbation Theory in Quantum Chromodynamics., 1977.

[9] W.J. Stirling. private communication. URL http://www.hep.ph.ic.ac.uk/~wstirlin/plots/plots.html.

[10] F. Bloch and A. Nordsieck. Note on the radiation field of the electron, Jul 1937. URL https://link.aps.org/doi/10.1103/PhysRev.52.54.

[11] Toichiro Kinoshita. Mass singularities of feynman amplitudes, 1962. URL https://doi.org/10.1063/1.1724268.

[12] T. D. Lee and M. Nauenberg. Degenerate systems and mass singularities, Mar 1964. URL https://link.aps.org/doi/10.1103/PhysRev.133.B1549.

[13] A. Kulesza, G. Sterman, and W. Vogelsang. Electroweak vector boson production in joint resummation, 2002. URL https://arxiv.org/abs/hep-ph/0207148.

[14] Torbjörn Sjöstrand, Stefan Ask, Jesper R. Christiansen, Richard Corke, Nishita Desai, Philip Ilten, Stephen Mrenna, Stefan Prestel, Christine O. Rasmussen, and Peter Z. Skands. An introduction to pythia 8.2, Jun 2015. ISSN 0010-4655. URL http://dx.doi.org/10.1016/j.cpc.2015.01.024.

[15] Manuel Bähr, Stefan Gieseke, Martyn A. Gigg, David Grellscheid, Keith Hamilton, Oluseyi Latunde-Dada, Simon Plätzer, Peter Richardson, Michael H. Seymour, Alexander Sherstnev, and Bryan R. Webber. Herwig++ physics and manual, Nov 2008. ISSN 1434-6052. URL http://dx.doi.org/10.1140/epjc/s10052-008-0798-9.

[16] T Gleisberg, S Hoeche, F Krauss, A Schaelicke, S Schumann, and J Winter. Sherpa 1. , a proof-of-concept version, Feb 2004. ISSN 1029-8479. URL http://dx.doi.org/10.1088/1126-6708/2004/02/056.

[17] E. Boos, M. Dobbs, W. Giele, I. Hinchliffe, J. Huston, V. Ilyin, J. Kanzaki, K. Kato, Y. Kurihara, L. Lonnblad, M. Mangano, S. Mrenna, F. Paige, E. Richter-Was, M. Seymour, T. Sjostrand, B. Webber, and D. Zeppenfeld. Generic user process interface for event generators, 2001.

[18] Stefano Catani, Frank Krauss, Bryan R Webber, and Ralf Kuhn. Qcd matrix elements + parton showers. *Journal of High Energy Physics*, 2001(11):063–063, Nov 2001. ISSN 1029-8479. doi: 10.1088/1126-6708/2001/11/063. URL http://dx.doi.org/10.1088/1126-6708/2001/11/063.

[19] Stefano Frixione and Bryan R Webber. Matching nlo qcd computations and parton shower simulations. *Journal of High Energy Physics*, 2002(06):029–029, Jun 2002. ISSN 1029-8479. doi: 10.1088/1126-6708/2002/06/029. URL http://dx.doi.org/10.1088/1126-6708/2002/06/029.

[20] Stefano Frixione, Paolo Nason, and Bryan R Webber. Matching nlo qcd and parton showers in heavy flavour production. *Journal of High Energy Physics*, 2003(08):007–007, Aug 2003. ISSN 1029-8479. doi: 10.1088/1126-6708/2003/08/007. URL http://dx.doi.org/10.1088/1126-6708/2003/08/007.

[21] Stefano Frixione and Bryan R. Webber. The mc@nlo 3.1 event generator, 2005.

[22] Rikkert Frederix and Stefano Frixione. Merging meets matching in MC@NLO. *JHEP*, 12:061, 2012. doi: 10.1007/JHEP12(2012)061.

[23] Victor S. Fadin. BFKL resummation. *Nucl. Phys. A*, 666:155–164, 2000. doi: 10.1016/S0375-9474(00)00022-1.

[24] I. I. Balitsky and L. N. Lipatov. The Pomeranchuk Singularity in Quantum Chromodynamics. *Sov. J. Nucl. Phys.*, 28:822–829, 1978.

[25] Richard D. Ball, Valerio Bertone, Stefano Carrazza, Luigi Del Debbio, Stefano Forte, Patrick Groth-Merrild, Alberto Guffanti, Nathan P. Hartland, Zahari Kassabov, José I. Latorre, Emanuele R. Nocera, Juan Rojo, Luca Rottoli,

Emma Slade, and Maria Ubiali. Parton distributions from high-precision collider data. *The European Physical Journal C*, 77(10), Oct 2017. ISSN 1434-6052. doi: 10.1140/epjc/s10052-017-5199-5. URL http://dx.doi.org/10.1140/epjc/s10052-017-5199-5.

[26] FRANK SIEGERT. Monte-carlo event generation for the lhc, 2010. URL http://etheses.dur.ac.uk/484/.

[27] B. Andersson, G. Gustafson, G. Ingelman, and T. Sjöstrand. Parton fragmentation and string dynamics. *Physics Reports*, 97(2):31–145, 1983. ISSN 0370-1573. doi: https://doi.org/10.1016/0370-1573(83)90080-7. URL https://www.sciencedirect.com/science/article/pii/0370157383900807.

[28] Torbjorn Sjostrand. Jet Fragmentation of Nearby Partons. *Nucl. Phys. B*, 248: 469–502, 1984. doi: 10.1016/0550-3213(84)90607-2.

[29] Underlying Event Measurements with Leading Particles and Jets in pp collisions at $\sqrt{s} = 13$ TeV. Technical report, CERN, Geneva, 2015. URL https://cds.cern.ch/record/2104473.

[30] Serguei Chatrchyan et al. Measurement of the underlying event in the Drell-Yan process in proton-proton collisions at $\sqrt{s} = 7$ TeV. *Eur. Phys. J. C*, 72: 2080, 2012. doi: 10.1140/epjc/s10052-012-2080-4.

[31] A. M. Sirunyan et al. Measurement of the underlying event activity in inclusive Z boson production in proton-proton collisions at $\sqrt{s} = 13$ TeV. *JHEP*, 07:032, 2018. doi: 10.1007/JHEP07(2018)032.

[32] Albert M. Sirunyan et al. Study of the underlying event in top quark pair production in pp collisions at 13 TeV. *Eur. Phys. J. C*, 79(2):123, 2019. doi: 10.1140/epjc/s10052-019-6620-z.

[33] Florian Bechtel. *The underlying event in proton-proton collisions*. PhD thesis, Hamburg U., 2009.

[34] Albert M Sirunyan et al. Extraction and validation of a new set of CMS PYTHIA8 tunes from underlying-event measurements. *Eur. Phys. J. C*, 80(1):4, 2020. doi: 10.1140/epjc/s10052-019-7499-4.

[35] A. Banfi, S. Redford, M. Vesterinen, P. Waller, and T. R. Wyatt. Optimisation of variables for studying dilepton transverse momentum distributions at hadron colliders. *Eur. Phys. J. C*, 71:1600, 2011. doi: 10.1140/epjc/s10052-011-1600-y.

[36] Albert M Sirunyan et al. Measurements of differential Z boson production cross sections in proton-proton collisions at $\sqrt{s} = 13$ TeV. *JHEP*, 12:061, 2019. doi: 10.1007/JHEP12(2019)061.

[37] Andy Buckley, Hendrik Hoeth, Heiko Lacker, Holger Schulz, and Jan Eike von Seggern. Systematic event generator tuning for the LHC. *Eur. Phys. J. C*, 65: 331–357, 2010. doi: 10.1140/epjc/s10052-009-1196-7.

[38] Stefano Carrazza and Marco Lazzarin. N3pdf/mcnntunes: mcnntunes 0.1.0, October 2020. URL https://doi.org/10.5281/zenodo.4071125.

[39] Marco Lazzarin, Simone Alioli, and Stefano Carrazza. MCNNTUNES: Tuning Shower Monte Carlo generators with machine learning. *Comput. Phys. Commun.*, 263:107908, 2021. doi: 10.1016/j.cpc.2021.107908.

[40] Martín Abadi, Ashish Agarwal, Paul Barham, Eugene Brevdo, Zhifeng Chen, Craig Citro, Greg S. Corrado, Andy Davis, Jeffrey Dean, Matthieu Devin, Sanjay Ghemawat, Ian Goodfellow, Andrew Harp, Geoffrey Irving, Michael Isard, Yangqing Jia, Rafal Jozefowicz, Lukasz Kaiser, Manjunath Kudlur, Josh Levenberg, Dandelion Mané, Rajat Monga, Sherry Moore, Derek Murray, Chris Olah, Mike Schuster, Jonathon Shlens, Benoit Steiner, Ilya Sutskever, Kunal Talwar, Paul Tucker, Vincent Vanhoucke, Vijay Vasudevan, Fernanda Viégas, Oriol Vinyals, Pete Warden, Martin Wattenberg, Martin Wicke, Yuan Yu, and Xiaoqiang Zheng. TensorFlow: Large-scale machine learning on heterogeneous systems, 2015. URL https://www.tensorflow.org/. Software available from tensorflow.org.

[41] F. Rosenblatt. The perceptron: A probabilistic model for information storage and organization in the brain. 1958. URL https://doi.org/10.1037/h0042519.

[42] Kurt Hornik. Approximation capabilities of multilayer feedforward networks. *Neural Networks*, 4(2):251–257, 1991. ISSN 0893-6080. doi: https://doi.org/10.1016/0893-6080(91)90009-T. URL https://www.sciencedirect.com/science/article/pii/089360809190009T.

[43] Moshe Leshno, Vladimir Ya. Lin, Allan Pinkus, and Shimon Schocken. Multilayer feedforward networks with a nonpolynomial activation function can approximate any function. *Neural Networks*, 6(6):861–867, 1993. ISSN 0893-6080. doi: https://doi.org/10.1016/S0893-6080(05)80131-5. URL https://www.sciencedirect.com/science/article/pii/S0893608005801315.

[44] Vardan Khachatryan et al. Pseudorapidity distribution of charged hadrons in proton-proton collisions at $\sqrt{s} = 13$ TeV. *Phys. Lett. B*, 751:143–163, 2015. doi: 10.1016/j.physletb.2015.10.004.

[45] Timo Antero Aaltonen et al. Study of the energy dependence of the underlying event in proton-antiproton collisions. *Phys. Rev. D*, 92(9):092009, 2015. doi: 10.1103/PhysRevD.92.092009.

[46] Measurement of the Underlying Event Activity at the LHC at 7 TeV and Comparison with 0.9 TeV. Technical report, CERN, Geneva, 2012. URL http://cds.cern.ch/record/1478982.

[47] Albert M. Sirunyan et al. Measurement of charged particle spectra in minimum-bias events from proton–proton collisions at $\sqrt{s} = 13\,\text{TeV}$. *Eur. Phys. J. C*, 78 (9):697, 2018. doi: 10.1140/epjc/s10052-018-6144-y.

[48] Nikolaus Hansen. The CMA evolution strategy: A tutorial. *CoRR*, abs/1604.00772, 2016. URL http://arxiv.org/abs/1604.00772.

[49] G. Cowan. *Statistical data analysis*. Oxford University Press, USA, 1998.

[50] Richard D. Ball et al. Parton distributions from high-precision collider data. *Eur. Phys. J. C*, 77(10):663, 2017. doi: 10.1140/epjc/s10052-017-5199-5.